Energy & Environmental Science
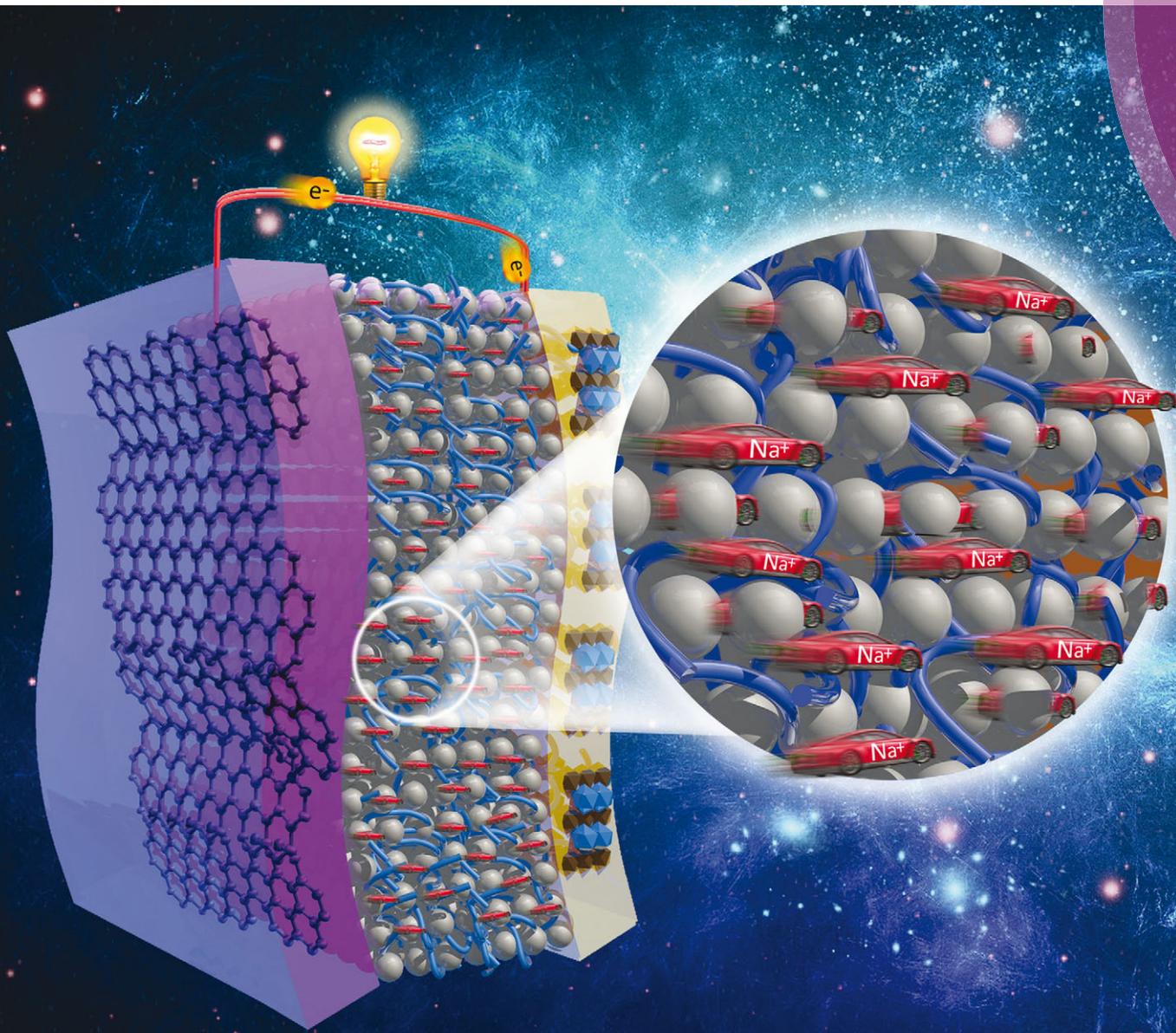
PAPER
Youngsik Kim *et al.*
A hybrid solid electrolyte for flexible solid-state sodium batteries

A hybrid solid electrolyte for flexible solid-state sodium batteries†

Jae-Kwang Kim,[a] Young Jun Lim,[a] Hyojin Kim,[a] Gyu-Bong Cho[b] and Youngsik Kim*[a]

Development of Na-ion battery electrolyte with high-performance electrochemical properties and high safety is still challenging to achieve. In this study, we report on a NASICON ($Na_3Zr_2Si_2PO_{12}$)-based composite hybrid solid electrolyte (HSE) designed for use in a high safety solid-state sodium battery for the first time. The composite HSE design yields the required solid-state electrolyte properties for this application, including high ionic conductivity, a wide electrochemical window, and high thermal stability. The solid-state batteries of half-cell type exhibit an initial discharge capacity of 330 and 131 mA h g^{-1} for a hard carbon anode and a $NaFePO_4$ cathode at a 0.2C-rate of room temperature, respectively. Moreover, a pouch-type flexible solid-state full-cell comprising hard carbon/HSE/$NaFePO_4$ exhibits a highly reversible electrochemical reaction, high specific capacity, and a good, stable cycle life with high flexibility.

Broader context

The considerable interest in Na-ion batteries has continued to increase as a result of their applicability to large-scale energy storage systems, and also because of the high abundance and uniform worldwide distribution of Na and its corresponding low cost compared to Li. However, safety issues related to the use of conventional combustible organic electrolytes in large-scale batteries for vehicle or grid applications are of great concern. It is anticipated that such safety issues can be fully addressed through the use of non-flammable solid electrolytes in solid-state batteries. However, the application of solid ceramic and polymer electrolytes in batteries has led to poor electrochemical performance, which is primarily due to the resultant high solid–solid interface resistance. Thus, a new electrolyte strategy is urgently required in order to overcome this problem. In this work, a NASICON ($Na_3Zr_2Si_2PO_{12}$) ceramic-based hybrid solid electrolyte (HSE) is proposed and shown to exhibit high electrochemical performances as a result of its decreased interface resistance, high thermal stability, and high electrochemical stability. Using the HSE, a flexible pouch-type full cell of hard carbon/HSE/$NaFePO_4$ is assembled for the first time, exhibiting good and stable cycle performance with a high capacity.

Introduction

Sodium (Na) batteries are attracting increasing attention as potentially low-cost, environmentally friendly technology for use in large-scale applications, such as in electric vehicles (EVs) and energy storage systems (ESS). Na possesses several advantages including low cost, natural abundance, and low resource toxicity. In principle, the reversible Na-ion intercalation mechanisms of the Na electrode materials used in Na-ion batteries are very similar to those of lithium (Li)-ion batteries. In addition, the voltage and cycling stability of Na electrode materials are competitive with those of Li electrode materials.[1–5] However, currently reported organic liquid electrolytes for use in Na batteries do not properly satisfy both the cathode and anode requirements, as high-performance electrochemical properties must be obtained.[6–9] In addition, the use of flammable liquid electrolytes in Na-ion batteries raises safety concerns as in the case of Li-ion batteries. The safety issues related to the use of conventional combustible organic electrolytes are of great concern in large batteries for vehicle or grid applications. It is anticipated that such safety issues can be fully addressed through the use of solid-state batteries, because of the non-flammability of solid electrolytes. For the solid electrolytes, solid-phase materials such as Na-ion conductive ceramics, polymers, or ceramic and polymer composites have been considered

[a] School of Energy & Chemical Engineering, Ulsan National Institute of Science and Technology (UNIST), Ulsan 689-798, Republic of Korea. E-mail: ykim@unist.ac.kr
[b] School of Materials Science and Engineering, Gyeongsang National University, 900, Gajwa-dong, Jinju 660-701, Republic of Korea

† Electronic supplementary information (ESI) available: XRD, FT-IR, SEM-EDX, DSC, FT-Raman, Arrhenius plots, bond length of CF_3SO_3, shrinkage test, charge–discharge curves, photographs of a flexible solid-state Na battery, short-term cycling of flexible solid-state batteries with conducting and non-conducting ceramic. See DOI: 10.1039/c5ee01941a

This journal is © The Royal Society of Chemistry 2015

Energy Environ. Sci., 2015, **8**, 3589–3596 | 3589

as potential rechargeable battery electrolytes.[10–19] Ceramic solid electrolytes such as Na–β''-Al$_2$O$_3$ and NASICON (Na$_3$Zr$_2$Si$_2$PO$_{12}$) have several potential advantages, including a wide electrochemical window (>5 V), high thermal stability, no leakage or pollution, high ionic conductivity ($>10^{-4}$ S cm^{-1}) with a high cation transference number ($t \approx 1$), high resistance to shocks and vibrations, and the potential for easy miniaturization.[10–12] However, their electrochemical properties are poor in batteries, because of the high interfacial resistance between solid electrolytes and solid electrodes.[13–15] Moreover, the ceramic materials are too hard and brittle for flexible battery applications. On the other hand, solid polymer electrolytes such as poly(ethylene oxide) (PEO) have good mechanical properties like high flexibility and lightweight, but tend to exhibit low ionic conductivity ($<10^{-5}$ S cm^{-1} at room temperature) with a low cation transference number ($t = 0.2$–0.4) and poor oxidation resistivity.[16] To take advantage of the properties of both ceramics and polymers, an ion-conducting ceramic and a polymer composite has been considered as a potential electrolyte, which can provide improved ionic conductivity and cation transference number with high flexibility and suitable mechanical strength.[17–19] However, the composite electrolytes exhibit poor electrochemical properties, as a result of the solid electrode/solid electrolyte interfacial resistance problem.[20] Therefore, the development of a composite electrolyte with strongly beneficial physical and electrochemical properties and low solid–solid interface resistance remains a challenge.

Herein, we report on a NASICON-based composite hybrid solid electrolyte (HSE) designed for use in a high safety solid-state Na battery for the first time. The composite HSE design yields the required solid-state electrolyte properties for this application, including high ionic conductivity, a wide electrochemical window, low solid/solid interface resistance and high thermal stability. Test half-cells at room temperature exhibit initial discharge capacity values of 330 and 131 mA h g^{-1} for a hard carbon anode and a NaFePO$_4$ cathode at a 0.2C-rate, respectively; while a pouch-type flexible solid-state full-cell comprising hard carbon/HSE/NaFePO$_4$ exhibits a highly reversible electrochemical reaction, high specific capacity, and a good, stable cycle life with high flexibility.

Experimental

Preparation of Na-conducting hybrid solid electrolyte (HSE)

The NASICON-type Na$_3$Zr$_2$Si$_2$PO$_{12}$ solid electrolyte was prepared *via* a solid-state reaction method.[18] Powder Na$_3$PO$_4\cdot$12H$_2$O, SiO$_2$, and ZrO$_2$ were mixed and then calcined at 400 and 1100 °C. After a second mixing and calcining, the powder was sintered at 1230 °C. The NASICON ceramic powder and the PVdF–HFP polymer were mixed together using a Planetary Mills (700 rpm) in *N,N*-dimethylacetamide (DMAc) : acetone (1 : 2) solvent at room temperature for 30 h. The resultant viscous homogeneous solution was cast as a membrane on a Teflon mold with a doctor blade and then immersed in water for 10 min. The collected solid membrane was oven dried at 60 °C for 12 h and then vacuum dried at 70 °C for 6 h. The solid membrane was pressed in 2.8 MPa after drying. The HSE was prepared by soaking the

solid membrane for 3 min in a solution of 1 M sodium triflate/TEGDME followed by pressure application (6.3 kPa) to remove excess liquid electrolyte. The final weight percentage in HSE is 70 : 15 : 15 ($\pm$0.2) for NASICON ceramic : PVdF–HFP : ether-based electrolyte.
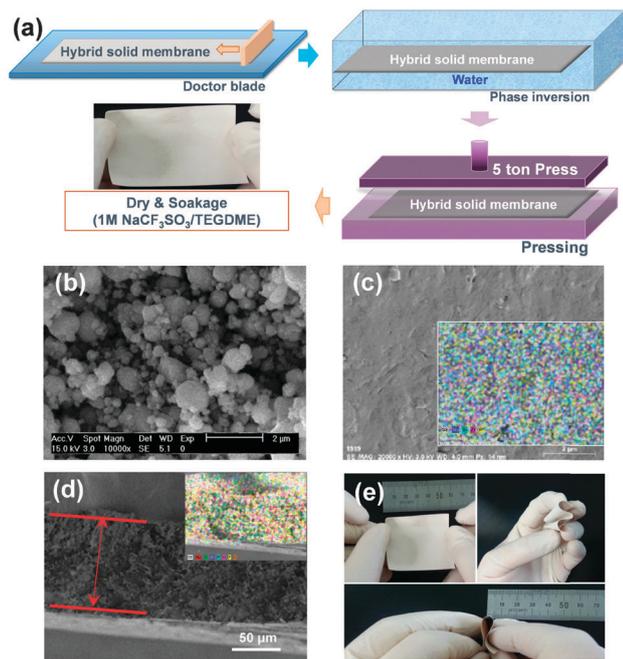
Electrochemical evaluation

Carbon-coated LiFePO$_4$ was synthesized using a modified mechanical activation method (carbon: 5 wt%) and was converted into NaFePO$_4$ *via* electrochemical ion exchange.[4] To prepare the cathode, the active material powder, carbon black, and the PVdF (Aldrich) binder were mixed in the ratio 83 : 7 : 10 by weight, and the resultant viscous slurry of the *N*-methyl pyrrolidone (NMP) solvent was cast on carbon paper and dried at 95 °C under vacuum for 12 h. Also, to prepare the hard carbon anode, the active material powder, carbon black, and poly(vinylidene fluoride) (PVdF: Aldrich) binder were mixed in the ratio 80 : 10 : 10 by weight, and the resultant viscous slurry in *N*-methyl pyrrolidone (NMP) solvent was cast on carbon paper and dried at 95 °C under vacuum for 12 h. The electrode films were cut into 35 cm^2 portions (5 cm × 7 cm) for the pouch-type cells. The pouch-type flexible solid-state Na cells were fabricated using a hard carbon anode and a NaFePO$_4$/C cathode with Na-conducting HSE without a separator. The cell assembly was performed in an argon atmosphere in a glove box (H$_2$O < 10 ppm). The charge–discharge and cycling properties were evaluated and found to be between 1.5 and 4.0 V at 0.2, 0.5, and 1C-rate current density using an automatic galvanostatic charge–discharge unit (WonA Tech. Co.) at room temperature.

Instrumentation

The crystal structure of the cathode material was characterized *via* XRD (SIEMENS D5005) data using Cu Kα radiation (35 mA/40 kV). The FT-IR absorption spectra were recorded with a FT interferometer (VERTEX 80v, Bruker Optics). TGA of all materials was performed on a SDT-Q600 (USA) instrument under an oxygen flow at a heating rate of 10 °C min^{-1}. SEM and EDX mapping by field emission scanning electron microscopy (Philips XL30 S FEG) were employed to evaluate the particle size and homogeneity of the chemical composition. The ionic conductivities of the HSE and the ether-based liquid electrolyte were measured from −10 °C to 90 °C in a gold-plated cell, at a frequency range of 10^{-1}–10^6 Hz using a Novocontrol broadband dielectric spectrometer. The impedance spectroscopy was measured using a Solartron 1470E, over a frequency range of 10^{-2}–10^6 Hz. *Ab initio* Hartree–Fock (HF) self-consistent field (SCF) molecular orbital calculations were performed for the free and interacted CF$_3$SO$_3$ anions using the standard 6-31G* basis set. The electrochemical stability was determined *via* LSV of the Na/HSE/SS cells at a scan rate of 0.2 mV s^{-1} over the 2–7 V range at 25 °C. Sodium ion transference numbers (t_+) were measured using the D.C. polarization method with Bruce and Vincent correction. The frequency range for the EIS measurements was 500 kHz–100 MHz, with a 10 mV ac signal. Polarization was performed with a 20 mV dc signal.

3590 | *Energy Environ. Sci.*, 2015, **8**, 3589–3596

This journal is © The Royal Society of Chemistry 2015

Fig. 1 (a) HSE hybrid preparation process, involving NASICON powder, PVdF–HFP, and 1 M $NaCF_3SO_3$/TEGDME. (b) SEM images of NASICON powder, (c) HSE, and (d) cross-sectional HSE. (c and d, inset) EDX mapping of HSE and cross-sectional HSE. (e) Mechanical and flexible properties of HSE.

Results and discussion

To obtain high electrochemical performance solid-state batteries at room temperature, we focus on decreasing the solid/solid interface resistance of a composite electrolyte while attempting to retain its advantageous features, leading to the design of a ceramic–polymer–liquid composite electrolyte for use in solid-state Na batteries. The Na-conducting HSE, prepared *via* a hybrid process involving the doctor-blade method and phase inversion (Fig. 1a), is composed of Na-conducting NASICON ceramic powder, a poly(vinylidene fluoride–hexafluoropropylene) (PVdF–HFP) binder, and 1 M sodium triflate ($NaCF_3SO_3$)/TEGDME liquid electrolyte in a 70 : 15 : 15 (±0.2) weight percentage. The PVdF–HFP polymer binder adds flexibility to the HSE and the small amount of ether-based liquid electrolyte decreases the solid/solid interfacial resistance and improves the ionic conductivity without liquid leakage. Instead of exhibiting a mixed performance, with some high- and low-performing characteristics, the HSE exhibits unique properties such as a high Na transference number (t_{Na}), high electrochemical stability, and increased thermal stability. This leads to electrochemical and thermal improvement in the Na batteries in which this electrolyte is used.

The crystal structure of the NASICON ceramic powder, which is prepared *via* a solid-state reaction, is consistent with that of a standard ordered monoclinic *C*2/*c* space group.[21,22] The calculated NASICON lattice parameters are $a = 15.675$ Å, $b = 9.068$ Å, and $c = 9.223$ Å, and the X-ray diffraction (XRD) peak intensities are high and sharp, implying high crystallinity (crystallite size: 396.45 μm) with no impurities (Fig. S1, ESI†). The prepared

NASICON powder size ranges between 300 nm and 1 μm and the average particle size is estimated to be 700 nm, using scanning electron microscopy (SEM) (Fig. 1b). In XRD and Fourier transform infrared (FT-IR) spectroscopy analyses (Fig. S2, ESI†), the NASICON, PVdF–HFP, and 1 M $NaCF_3SO_3$/TEGDME exhibit a stable phase with no undesirable reactions during the hybrid preparation process. SEM images of HSE and cross-sectional HSE specimens are shown in Fig. 1c and d, respectively. It should be noted that, under application of a 2.8 MPa pressure, the HSE maintains a smooth surface with increased density (the thickness decreases from 200 to 100 μm). The morphologies of the HSE exhibit no obvious changes, and no significant aggregation of the NASICON particles is observed in the images (energy dispersive X-ray (EDX) image; Fig. 1c, inset). This result suggests that the NASICON powder and the PVdF–HFP polymer are homogeneously distributed in the HSE, forming a composite film. To confirm the homogenous atomic distribution of the NASICON and polymer in the HSE, EDX mappings and corresponding SEM images of the HSE are obtained, which are presented in Fig. 1d. The EDX data indicate uniform distributions of both the Na of the NASICON and the C atoms of the PVdF–HFP throughout the HSE sample. In addition, the spatial distributions of Na, Si, O, and P are well matched (Fig. S3, ESI†). The results verify that the NASICON powder and PVdF–HFP are homogeneously distributed in the HSE. The homogeneous distribution of the PVdF–HFP binder facilitates the beneficial mechanical properties and high flexibility of the material. Macroscopically, the entire HSE sample exhibits good mechanical properties with regard to flexibility, and can be bent, twisted, and even rolled up without cracking (Fig. 1e). It is apparent that the HSE has potential application in flexible solid-state Na batteries.

Electrochemical impedance spectroscopy (EIS) analyses are used to examine the interface and boundary stability, as shown in Fig. 2a. The spectra are in the form of a semi-circle with the real axis intercepts occurring at the lower frequency end; this corresponds to the total resistance, including the grain and interfacial resistances. The total resistance values of the NASICON + PVdF–HFP composite film, liquid electrolyte, and HSE are 9170, 148, and 1215 Ω, respectively. The liquid electrolyte has the lowest total resistance because of the compact contact through absorption into the electrode. On the NASICON + PVdF–HFP composite film, the incorporation of the polymer creates a new boundary between the NASICON ceramic and PVdF–HFP polymer, resulting in high total resistance with high boundary resistance. The total resistance of the HSE is significantly lower than those of the NASICON + PVdF–HFP film and the previously reported solid electrolytes. This is because the inclusion of the small amount of liquid electrolyte in the HSE improves the ceramic–ceramic, ceramic–polymer, and electrolyte–electrode interface stabilities.[13,23–25] The interface is important in solid-state batteries, as it determines the Na insertion reversibility and the cycling and rate capability. Although the total resistance value of HSE is higher than that of liquid electrolyte, it is still possible to achieve high reversible capacity and cycling stability at room temperature.
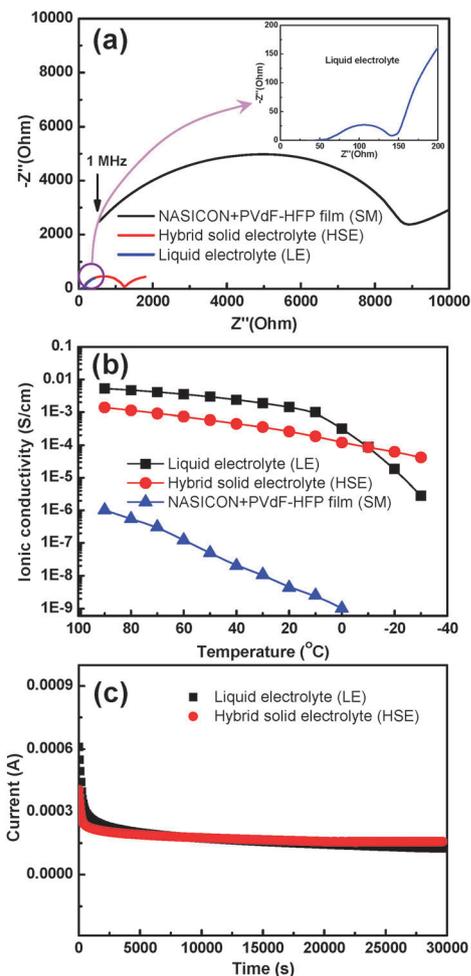
This journal is © The Royal Society of Chemistry 2015

Energy Environ. Sci., 2015, 8, 3589–3596 | 3591

Fig. 2 (a) EIS for composite solid film, HSE, and ether-based liquid electrolyte (inset), respectively. (b) Ionic conductivity vs. temperature profile for composite solid film (SM), HSE, and ether-based liquid electrolyte (LE), respectively. (c) Chronoamperometry results for LE and HSE.

Fig. 2b shows the ionic conductivities of the HSE, NASICON + PVdF–HFP film, and ether-based liquid electrolyte as a function of temperature. The high total resistance (Fig. 2a) of the composite film significantly decreases the ionic conductivity to 1.1×10^{-8} S cm^{-1} at 30 °C. In contrast, the Na-conducting HSE achieves a high ionic conductivity of 1.2×10^{-4} S cm^{-1} at 0 °C, which increases monotonically with increasing temperature over the entire investigated temperature range (up to 1.4×10^{-3} S cm^{-1} at 90 °C). The conductivity values for each temperature are higher than those reported for ceramic-based solid electrolyte and are close to those reported for gel polymer electrolytes.[23,25–28] This is because of the improved boundary stability obtained via the incorporation of the small amount of liquid electrolyte in the HSE. Furthermore, the amorphous domain of the PVdF–HFP increases with the addition of liquid electrolyte, which facilitates greater ion mobility.[29] Below 10 °C, the conductivity of the ether-based liquid electrolyte also decreases rapidly, due to crystallization of the TEGDME solvent (Fig. S4, ESI†). However, the HSE maintains a high ionic conductivity ($>10^{-4}$ S cm^{-1}) at low temperature. The incorporation of the NASICON and PVdF–HFP degrades the phase

transition and crystallization of the liquid electrolyte, resulting in improved low-temperature conductivity. The inhibition of phase transition and crystallization of the liquid electrolyte compensates for the low ionic mobility otherwise imposed by the polymer and ceramic particles at these temperatures.[30,31] The temperature dependence of the HSE conductivity exhibits the typical Arrhenius behavior for solid electrolytes and is well described by the Arrhenius equation (eqn (1)):[32,33]

$$\sigma = \frac{A}{T}\exp\left(-\frac{E_a}{kT}\right) \qquad (1)$$

where $\sigma(T)$ is the conductivity (S cm^{-1}), A is the pre-exponential factor, E_a is the activation energy, k is the Boltzmann constant, and T is the temperature (K). This indicates that the ionic conduction mechanism primarily involves Na$^+$, because of the interfacial interactions occurring on the ceramic grain boundaries, which are connected with the liquid electrolyte anion trapping.[29,30,34] The occurrence of the interfacial interaction is supported by FT-Raman analysis of the ν_sSO$_3$ mode, in which the anion trapping of the ceramic particles is evidenced by a decrease in the concentration of the Na$^+$-coordinated CF$_3$SO$_3$ anions (Fig. S5, ESI†). The Arrhenius plots of ionic conduction for the liquid electrolyte, NASICON + PVdF–HFP film, and the HSE are shown in Fig. S6 (ESI†). From the plot of $\ln(\sigma T)$ vs. $1000T^{-1}$, the total E_a is calculated to be 0.18 eV for the ether-based liquid electrolyte, 0.99 eV for the composite film, and 0.23 eV for the HSE, respectively. The NASICON + PVdF–HFP composite film exhibits higher total E_a, which indicates the high energy required to initiate the electrochemical process or charge transport. This means that the incorporation of the polymer gives a higher activation barrier for interfacial cation transfer. The total HSE activation energy is similar to that of the liquid electrolyte, although the HSE ionic conductivity is lower. This indicates that the charge transfer and Na diffusion at the interface occur rapidly in the HSE, as in the liquid electrolyte. This rapid charge transfer and Na diffusion are due to the formation of an ionically conducting liquid medium (also referred to as solidified liquid) on the ceramic and polymer surfaces via NASICON Na-ion hopping. This occurs as a result of the interfacial interaction and the consequential splitting of the Na$^+$ and CF$_3$SO$_3$ ion pairing.[29–31,35–37] Accordingly, the charge–discharge performance of a solid-state Na battery with HSE is comparable to that of a battery incorporating liquid electrolyte, and superior to that of a solid polymer electrolyte battery.

The transference numbers (t_{Na}) of the Na$^+$ ions are estimated by chronoamperometry, as shown in Fig. 2c. The calculated t_{Na} obtained by comparing the maximum and equilibrium current values are 0.43 and 0.92 for the ether-based liquid electrolyte and HSE, respectively. As a result, the practical ionic conductivity of Na ions for the HSE is considerably larger than that of the liquid electrolyte when the same amount of liquid electrolyte is used. This may be because of contributions from the Na-conducting NASICON solid electrolyte and anion trapping, which promote the movement of free Na ions. This experimental evidence could add credence to the contribution of the Na-conducting ceramic solid electrolyte in
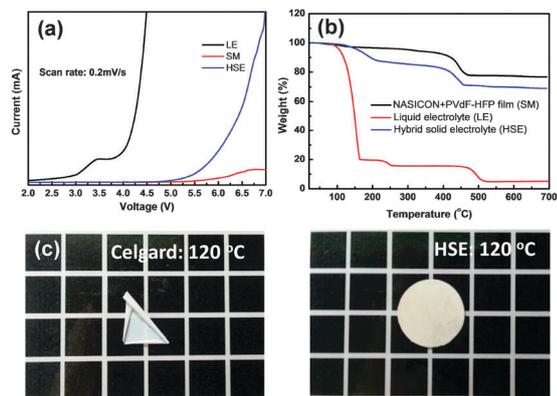
3592 | Energy Environ. Sci., 2015, **8**, 3589–3596

This journal is © The Royal Society of Chemistry 2015

Fig. 3 (a) LSV and (b) TGA results for the composite solid film, ether-based liquid electrolyte (1 M NaCF$_3$SO$_3$/TEGDME), and HSE. (c) Shrinkage of commercial membrane (Celgard) and HSE at 120 °C.

HSE for the ion transport mechanism. Also, the high HSE t_{Na} renders it attractive among the electrolyte materials considered in the current study.

The electrochemical stability of HSE is an important parameter for establishing its satisfactory performance in Na batteries. Fig. 3a shows the linear sweep voltammograms (LSV) of Na/HSE/SS cells obtained at a scan rate of 0.2 mV s^{-1} from 2 to 7 V $vs.$ Na/Na$^+$. The NASICON + PVdF–HFP composite film exhibits high electrochemical stability up to 6.0 V, which can be ascribed to the decomposition of the PVdF–HFP.[38] A low background current is measured in the potential region between 2.0 and 3.0 V for the ether-based liquid electrolyte, whereas the HSE current is almost zero between 2.0 and 5.0 V. The small ether-based electrolyte background current may be attributed to the change in the stainless steel surface.[39] The ether-based electrolyte exhibits low electrochemical stability windows of approximately 3.0 V, but the HSE has high electrochemical oxidation stability up to 5.0 V, although this is affected by a high loading of the NASICON ceramic. The high loading of NASICON with a small amount of liquid electrolyte corresponds to a large liquid medium ratio, which affects the interfacial interaction. In the liquid medium on the NASICON particle surfaces, the bonding distance for each atom is decreased in comparison with that of the free CF$_3$SO$_3$ anions (Fig. S7, ESI†). This means that the presence of the liquid medium also facilitates increased liquid molecular bonding strength, resulting in enhanced thermal and electrochemical stability.[29,34] Moreover, the polymer chain in the PVdF–HFP composite has a blocking effect, preventing decomposition of the adsorbed liquid electrolyte.[31] From the oxidation stability results, it can be concluded that HSE is more favorable for practical applications in high-voltage Na batteries.
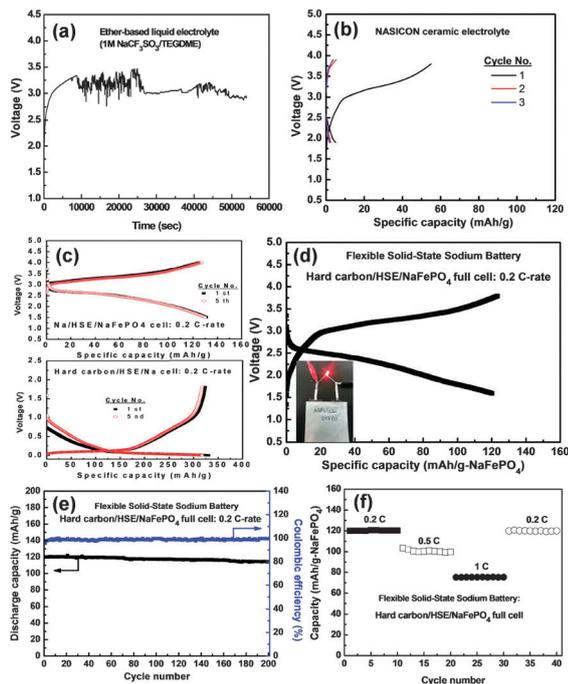
Thermal stability is crucial for the safety of Na batteries. The good thermal stability of HSE is revealed by Fig. 3b and the theoretical weight percentage corresponds well with thermogravimetric analysis (TGA) results. The initial decomposition of the ether-based electrolyte occurs at 150 °C, and 15 wt% of the liquid electrolyte in HSE is removed by 210 °C. The initial decomposition of the PVdF–HFP occurs at 400 °C and is completed at 460 °C with 13 wt% loss. The behavior of the

PVdF–HFP is the same as that of the liquid–electrolyte-free NASICON–PVdF–HFP composite film. 70 wt% of the dried NASICON powder is maintained at 700 °C, and 2 wt% ash from the PVdF–HFP is formed at 460 °C. However, the ether-based liquid electrolyte begins decomposition at 100 °C and exhibits poor thermal stability. The difference in the liquid electrolyte decomposition temperatures of the HSE and pure liquid phase is due to the liquid medium on the NASICON particle surfaces, which corresponds to the observed electrochemical stability. As stated above, the liquid medium has a stronger liquid molecular bond than that in the liquid electrolyte, resulting in an improvement of the electrochemical and thermal stability. Furthermore, the NASICON particle and the polymer binder apparently help to absorb and retain the liquid electrolyte inside the pores, reducing the tendency towards rapid evaporation.[40] The trapping of a small amount of liquid electrolyte inside the HSE may be beneficial from a practical point of view, because the small vapor pressure can obviate the risk of ignition. In shrinkage comparison tests against a commercial membrane (Celgard), the HSE exhibits good thermal stability against shrinkage, whereas the commercial membrane experiences shrinkage from 100 °C (Fig. 3c and Fig. S8, ESI†). During this thermal stability test, no shrinkage or degradation phenomena are observed in the HSE, because of its high ceramic content. Moreover, the HSE shows successful flame retarding ability and it does not catch fire when put in the flame without any shrinkage as shown in Fig. S9 (ESI†).

Electrochemical performance testing of the ether-based liquid electrolyte, ceramic solid electrolyte, and HSE is conducted using NaFePO$_4$ as a cathode and Na metal as an anode. The NaFePO$_4$ is prepared via electrochemical ion exchange, which is known to reversibly store Na ions within its structure at a voltage of < 2.8 V $vs.$ Na$^+$/Na.[4] The charge–discharge curves of the TEGDME based liquid electrolyte and ceramic solid electrolyte cells are displayed in Fig. 4a and b. The liquid electrolyte is not charged to 4.0 V (Fig. 4a), because of its low electrochemical stability (Fig. 3a). Furthermore, the electrochemical behavior of the cell with the NASICON ceramic solid electrolyte is not reversible (Fig. 4b). As can be seen in Fig. 4b, the first charge capacity curve smoothly reaches 57 mA h g^{-1}. After the first charge, however, the subsequent cycles rapidly drop to below 5 mA h g^{-1}. This is due to the increased interfacial resistance between the NaFePO$_4$ electrode and NASICON electrolyte during charging, which is in turn caused by the change in the electrode volume that occurs during extraction/insertion of the Na ions. The increase in the interfacial resistance also occurs because the NASICON ceramic electrolyte cannot compensate for the empty space between the electrode and electrolyte.[41] The increased interfacial resistance indicates that the ceramic solid electrolyte cell has poor cyclability. A NASICON + PVdF–HFP composite cell is also assembled and tested, but does not exhibit any reasonable voltage curve at the same current rate because of the high interfacial resistance.

Fig. 4c (top) shows the voltage profiles obtained for the first cycle for a Na/HSE/NaFePO$_4$ half-cell. With a 131 mA h g^{-1} discharge capacity, a 2% irreversible capacity between charge

This journal is © The Royal Society of Chemistry 2015

Energy Environ. Sci., 2015, 8, 3589–3596 | 3593

Fig. 4 Charge–discharge curves of (a) ether-based liquid electrolyte and (b) NASICON solid electrolyte cells with a NaFePO$_4$ cathode. (c) Charge–discharge curves of a half-cell for hard carbon/HSE/Na and Na/HSE/NaFePO$_4$, respectively. (d) Initial charge–discharge curve, (e) cycle performances and Coulombic efficiency of a flexible full-cell for hard carbon/HSE/NaFePO$_4$ batteries ((d, inset) tested pouch-type full cell, room temperature. 0.2C-rate). (f) Short-term cycling of a flexible solid-state Na cell with HSE at different C-rates (10 cycles at each C-rate, 25 °C, 1.5–4.0 V).

and discharge is observed during the first cycle. After the first cycle, reversible voltage curves with slopes of 2.7 V *vs.* Na$^+$/Na are continually maintained, corresponding to reversible Na-ion storage in the NaFePO$_4$ olivine structure during cycling. We also investigate the charge–discharge performance of the hard carbon anode with the HSE in a half-cell, as shown in Fig. 4c (bottom). The potentiogram slopes from 0.8 to 0.1 V during the initial reduction, followed by a long flat region between 0.1 and 0 V that reaches 330 mA h g^{-1}. During the subsequent oxidation, a capacity of ∼160 mA h g^{-1} is observed close to 0 V *vs.* Na/Na$^+$. Then, the potential gradually increases to 1.1 V, suggesting that the hard carbon anode undergoes a reversible sodiation; this irreversible capacity is determined to be 6 mA h g^{-1}. The irreversible capacity of the hard carbon in the HSE cell is significantly lower than that of the liquid electrolytes. Indeed, the irreversible capacities of the carbonate- and ether-based electrolytes are ∼60 and ∼30 mA h g^{-1} at 0.2C-rate, respectively (Fig. S10, ESI†).

The electrochemical properties of the full cell are observed using a flexible solid-state Na battery. The configuration of the proposed flexible solid-state Na battery, comprising a hard carbon anode/HSE/NaFePO$_4$ cathode, is shown in Fig. S11 (ESI†). Carbon paper is used as flexible current collector at both the anode and cathode. From the half-cell voltage curves of the Na/hard carbon and Na/NaFePO$_4$, the full-cell voltage curves of the hard carbon/HSE/NaFePO$_4$ can be predicted, and

correspond well to the slope voltage curves of the pouch-type hard carbon/NaFePO$_4$ flexible full-cell measured and depicted in Fig. 4d. The first cycle of the flexible full-cell shows 98% Coulombic efficiency. The 2% irreversible capacity may be related to the transfer of some Na$^+$ ions into the hard carbon anode or HSE. Furthermore, the discharge voltage is continually maintained with cycling, because of the stable contact between the electrode and HSE. The Coulombic efficiency of the full-cell is clearly improved after the first cycle to ∼100%, as shown in Fig. 4e. The hard carbon/HSE/NaFePO$_4$ full cell has an average voltage of ∼2.6 V, and yields a discharge capacity of ∼120 mA h g^{-1} at a 0.2C-rate. It also exhibits good capacity retention of 96% after 200 cycles (Fig. 4e). The flexible Na battery displays good rate-capability, comparable to that of a solid-state battery. The short-term cycling performance (10 cycles each at different C-rates) of the hard carbon/HSE/NaFePO$_4$ full cell is shown in Fig. 4f. The capacity drops with an increase in the current density, indicating that the capacity loss is restricted by Na ion diffusion. At each current density value, NaFePO$_4$ delivers reversible discharge capacities of 103.1 mA h g^{-1} at 0.5C and 75.4 mA h g^{-1} at 1C. The performance of the full cell at 0.2C-rate after subjecting it to 1C is almost identical to its initial behavior at 0.2C, indicating that the interfacial characteristics between the electrodes and HSE are quite stable during cycling. The HSE used in flexible batteries must maintain electrical isolation between the electrodes to prevent internal short circuiting, because flexible and bendable batteries are vulnerable to degradation of this isolation. Fig. S12 (ESI†) shows that the flexible solid-state Na cell can successfully illuminate a red LED lamp under both normal static and bent conditions. When the solid cell is manually bent several times, the solid Na cell lamp continues to receive power. Here, it is worth noting that the improved flexibility and bendability of the solid Na battery incorporating the HSE is consistent with the good mechanical deformability of the HSE.

Fig. 5 illustrates the mechanism by which incorporation of Na-conducting ceramic particles affects the ionic conductivity and t_{Na}. On the HSE, three Na-ion transport mechanisms are possible: (1) ceramic ion hopping; (2) plasticizer transport of liquid electrolyte; and (3) cross direction.[37,42] NASICON ceramic solid electrolyte has a high t_{Na} ($\approx$1), and the high loading of Na-conducting NASICON ceramic particles improves the t_{Na} through ion hopping between the ceramic particles, which is
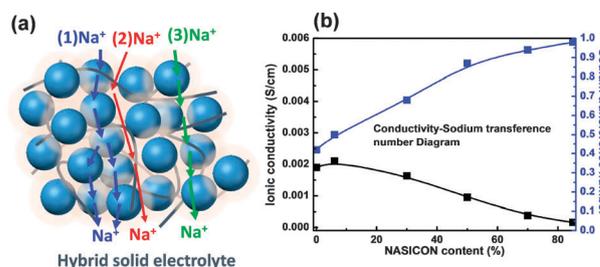
Fig. 5 (a) Model representation of the composite in HSE with Na-ion conducting paths. (b) Schematic representation of conductivity and Na transference number, which are contributed by ion hopping and plasticizer ion transport.

3594 | *Energy Environ. Sci.*, 2015, **8**, 3589–3596

This journal is © The Royal Society of Chemistry 2015

even slower than in the liquid medium surrounding the ceramic particles. This medium is created when the ceramic particles are in contact with each other and the absorbed liquid electrolyte forms a liquid shell. The plasticizer ion transport in the liquid shell is faster than the ceramic ion hopping, and the Na ion motion progresses more easily than that of the CF_3SO_3 anions, because the high loading of the ceramic particles hinders the movement of large anions through anion trapping.[35,40] This can be seen from the increased t_{Na}. The third Na ion transport pathway is the cross direction, as mentioned above, which involves passing through the ceramic and liquid phase. Cross ion transport has been reported in previous studies on polymer–ceramic and ceramic–liquid composite electrolytes.[20,43] The ion-hopping process is more favorable in high-content ceramics because of the Na-conducting pathway in NASICON particles. Also, the observed discharge capacity at different currents clarifies the contribution of the NASICON ceramic to the ion transference (Fig. S13, ESI†). Na transference occurs along the liquid electrolyte shell on the surface of the ceramic particle at low current density, but at high current density, the Na-conducting ceramic must join the Na ion transference because of the strong ion force for transport. The discharge capacities of non-Na-conducting HSE using Al_2O_3 ceramic and Na-conducting HSE using NASICON ceramic have been compared according to current density. The two HSE samples exhibit almost identical capacity at low current densities of 0.2 and 0.5C, but the discharge capacities at a high current density of 1C differ significantly, because of the contribution of the Na-conducting ceramic. The detailed mechanism responsible for the Na transport in certain types of HSE therefore requires further confirmation.

Conclusions

We have reported a novel kind of flexible solid-state Na battery configuration involving Na-conducting hybrid solid electrolyte (HSE). The HSE was prepared via a hybrid process and exhibited homogeneous distributions of NASICON ($Na_3Zr_2Si_2PO_{12}$) ceramic powder and PVdF–HFP polymer. After the preparation of a NASICON + PVdF–HFP composite film, a small amount of ether-based electrolyte was incorporated into the HSE to overcome the solid–solid interface problem. The composite design of the HSE resulted in advantageous solid-state electrolyte properties, which can satisfy the multiple requirements for use in flexible solid-state Na batteries, such as high ionic conductivity, a wide electrochemical window, and high thermal stability. The HSE exhibited high thermal stability against shrinkage and a high ionic conductivity of 3.6×10^{-4} S cm^{-1}, especially at room temperature. The Na transference number of HSE was higher than that of ether-based liquid electrolyte, at 0.92, and a good electrochemical stability window of 5.0 V vs. Na/Na$^+$ was achieved via the incorporation of the Na-conducting NASICON ceramic. Test half-cells were found to carry initial discharge capacity values of 330 mA h g^{-1} for a hard carbon anode and 131 mA h g^{-1} for a NaFePO$_4$ cathode at a 0.2C-rate. A pouch-type flexible solid-state full-cell of hard carbon/HSE/NaFePO$_4$

exhibited a highly reversible electrochemical reaction, high specific capacity, and a good, stable cycle life with high flexibility. The characteristic electrochemical properties of the Na-conducting HSE introduce new possibilities for their application in flexible electronic devices as a flexible power source.

Acknowledgements

Notes and references

1 B. L. Ellis and L. F. Nazar, *Curr. Opin. Solid State Mater. Sci.*, 2012, **16**, 168–177.

2 S. Komaba, W. Murata, T. Ishikawa, N. Yabuuchi, T. Ozeki, T. Nakayama, A. Ogata, K. Gotoh and K. Fujiware, *Adv. Funct. Mater.*, 2011, **21**, 3859–3867.

3 P. Barpanda, G. Oyama, S. Nishimura, S. C. Chung and A. Yamada, *Nat. Commun.*, 2014, **5**, 4358.

4 I. Hasa, D. Buchholz, S. Passerini, B. Scrosati and J. Hassoun, *Adv. Energy Mater.*, 2014, **4**, 1400083.

5 E. Lee, J. Lu, Y. Ren, X. Luo, X. Zhang, J. Wen, D. Miller, A. DeWahl, S. Hackney, B. Key, D. Kim, M. D. Slater and C. S. Johnson, *Adv. Energy Mater.*, 2014, **4**, 1400458.

6 A. Ponrouch, E. Marchante, M. Courty, J. M. Tarascon and M. Rosa Palacín, *Energy Environ. Sci.*, 2012, **5**, 8572–8583.

7 A. Ponrouch, A. R. Goñi and M. Rosa Palacín, *Electrochem. Commun.*, 2013, **27**, 85–88.

8 H. Kim, J. S. Park, S. H. Sahgong, S. Park, J. K. Kim and Y. Kim, *J. Mater. Chem. A*, 2014, **2**, 19584–19588.

9 H. Kim, J. Hong, Y. U. Park, J. Kim, I. Hwang and K. Kang, *Adv. Funct. Mater.*, 2015, **25**, 534–541.

10 G. B. Telnova and K. A. Solntsev, *Inorg. Mater.*, 2015, **51**, 257–266.

11 J. W. Fergus, *Solid State Ionics*, 2012, **227**, 102–112.

12 Y. Noguchi, E. Kobayashi, L. Plashnitsa, S. Okada and J. Yamaki, *Electrochim. Acta*, 2013, **101**, 59–65.

13 D. Santhanagopalan, D. Qian, T. McGilvray, Z. Wang, F. Wang, F. Camino, J. Graetz, N. Dudney and Y. S. Meng, *J. Phys. Chem. Lett.*, 2014, **5**, 298–303.

14 V. Palomares, P. Serras, I. Villaluenga, K. B. Hueso, J. Carretero-González and T. Rojo, *Energy Environ. Sci.*, 2012, **5**, 5884–5901.

15 H. D. Yoo, I. Shterenberg, Y. Gofer, G. Gershinsky, N. Pour and D. Aurbach, *Energy Environ. Sci.*, 2013, **6**, 2265–2279.

16 Y. Wang and W. H. Zhong, *ChemElectroChem*, 2015, **2**, 22–36.

17 Y. J. Wang, Y. Pan and D. Kim, *J. Power Sources*, 2006, **159**, 690–701.

18 Y. Kobayashi, H. Miyashiro, T. Takeuchi, H. Shigemura, N. Balakrishnan, M. Tabuchi, H. Kageyama and T. Iwahori, *Solid State Ionics*, 2002, **152–153**, 137–142.

19 K. Nairn, M. Forsyth, H. Every, M. Greville and D. R. MacFarlane, *Solid State Ionics*, 1996, **86–88**, 589–593.

20 Y. Inda, T. Katoh and M. Bab, *J. Power Sources*, 2007, **174**, 741–744.

21 J. K. Kim, F. Mueller, H. Kim, D. Bresser, J. S. Park, D. H. Lim, G. T. Kim, S. Passerini and Y. Kim, *NPG Asia Mater.*, 2014, **6**, e144.

22 J. K. Kim, E. Lee, H. Kim, C. Johnson, J. Cho and Y. Kim, *ChemElectroChem*, 2015, **2**, 328–332.

23 Y. Noguchi, E. Kobayashi, L. S. Plashnitsa, S. Okada and J. Yamaki, *Electrochim. Acta*, 2013, **101**, 59–65.

24 I. Seo and Y. Kim, *Solid State Ionics*, 2014, **261**, 106–110.

25 M. Haruta, S. Shiraki, T. Suzuki, A. Kumatain, T. Ohsawa, Y. Takagi, R. Shimizu and T. Hitosugi, *Nano Lett.*, 2015, **15**, 1498–1502.

26 J. B. Goodenough and Y. Kim, *Chem. Mater.*, 2010, **22**, 587–603.

27 J. Syzdek, M. Armand, M. Marcinek, A. Zalewska, G. Zukowska and W. Wieczorek, *Electrochim. Acta*, 2010, **55**, 1314–1322.

28 J. Y. Song, Y. Y. Wang and C. C. Wan, *J. Power Sources*, 1999, **77**, 183–197.

29 M. Osiňska, M. Walkowiak, A. Zalewska and T. Jesionowski, *J. Membr. Sci.*, 2009, **326**, 582–588.

30 A. J. Bhattacharyya and J. Maier, *Adv. Mater.*, 2004, **16**, 811–814.

31 J. K. Kim, L. Niedzicki, J. Scheers, C. R. Shin, D. H. Lim, W. Wieczorek, P. Johansson, J. H. Ahn, A. Matic and P. Jacobsson, *J. Power Sources*, 2013, **224**, 93–98.

32 M. G. Bellino, D. G. Lamas and N. E. Walsöe de Reca, *Adv. Mater.*, 2006, **18**, 3005–3009.

33 J. F. Ihlefeld, P. G. Clem, B. L. Doyle, P. G. Kotula, K. R. Fenton and C. A. Apblett, *Adv. Mater.*, 2011, **23**, 5663–5667.

34 J. K. Kim, J. Scheers, T. J. Park and Y. Kim, *ChemSusChem*, 2015, **8**, 636–641.

35 R. Blanga, D. Golodnitaky, G. Ardel, K. Freedman, A. Gladkich, Y. Rosenberg, M. Nathan and E. Peled, *Electrochim. Acta*, 2013, **114**, 325–333.

36 J. Y. Song, Y. Y. Wang and C. C. Wan, *J. Power Sources*, 1999, **77**, 183–197.

37 Y. Wang, W. H. Zhong, T. Schiff, A. Eyler and B. Li, *Adv. Energy Mater.*, 2015, **5**, 1400463.

38 Y. Liang, S. Cheng, J. Zhao, C. Zhang, S. Sun, N. Zhou, Y. Qiu and X. Zhang, *J. Power Sources*, 2013, **240**, 204–211.

39 A. C. Bloise, J. P. Donoso, C. J. Magon, A. V. Rosario and E. C. Pereira, *Electrochim. Acta*, 2003, **48**, 2239–2246.

40 Y. Zhu, F. Wang, L. Liu, S. Xiao, Z. Chang and Y. Wu, *Energy Environ. Sci.*, 2013, **6**, 618–624.

41 N. M. Asl, J. Keith, C. Lim, L. Zhu and Y. Kim, *Electrochim. Acta*, 2012, **79**, 8–16.

42 B. Kumar and L. G. Scanlon, *J. Power Sources*, 1994, **52**, 261–269.

43 Y. Lu, J. B. Goodenough and Y. Kim, *J. Am. Chem. Soc.*, 2011, **133**, 5756–5759.

3596 | *Energy Environ. Sci.*, 2015, **8**, 3589–3596

This journal is © The Royal Society of Chemistry 2015